**Molecular Origin of Enhanced Proton Conductivity in Anhydrous Ionic System**

*Zaneta Wojnarowska,[*,1,2] Krzysztof J. Paluch,[3] Evgeni Shoifet,[4,9] Christoph Schick,[4,9] Lidia Tajber,[5] Justyna Knapik,[1,2] Patryk Wlodarczyk,[6] Katarzyna Grzybowska,[1,2] Stella Hensel-Bielowka,[7] Sergey P. Verevkin,[8,9] and Marian Paluch[1,2]*

Corresponding Author *E-mail: zaneta.wojnarowska@us.edu.pl.

1. Institute of Physics, University of Silesia, Uniwersytecka 4, 40-007 Katowice, Poland

2. Silesian Center for Education and Interdisciplinary Research, 75 Pulku Piechoty 1A, 41-500 Chorzow, Poland

3. Centre for Pharmaceutical Engineering Science, Bradford School of Pharmacy, University of Bradford, Richmond Road, Bradford BD7 1DP, United Kingdom

4. Institute of Physics, University of Rostock, Wismarsche Straße 43−45, 18057 Rostock, Germany

5. School of Pharmacy and Pharmaceutical Sciences, Trinity College Dublin, College Green, Dublin 2, Ireland

6. Institute of Non-Ferrous Metals, ul. Sowinskiego 5, 44-100 Gliwice, Poland

7.Institute of Chemistry, University of Silesia, Szkolna 9, 40-006 Katowice, Poland

8. Institute of Physical Chemistry, University of Rostock, Dr.-Lorenz-Weg 1, 18059 Rostock, Germany

9. Faculty of Interdisciplinary Research, Department ‘‘Life, Light and Matter’’, University of Rostock, 18051 Rostock, Germany

**Abstract**

Ionic systems with enhanced proton conductivity are widely viewed as promising electrolytes in fuel cells and batteries. Nevertheless, a major challenge toward their commercial applications is determination of the factors controlling the fast proton hopping in anhydrous conditions. To address this issue, we have studied novel proton-conducting materials formed via a chemical reaction of lidocaine base with a series of acids characterized by a various number of proton-active sites. From ambient and high pressure experimental data, we have found that there are fundamental differences in the conducting properties of the examined salts. On the other hand, DFT calculations revealed that the internal proton hopping within the cation structure strongly affects the pathways of mobility of the charge carrier. These findings offer a

fresh look on the Grotthuss-type mechanism in protic ionic glasses as well as provide new ideas for the design of anhydrous materials with exceptionally high proton conductivity.

## Introduction

Over the past decades, the understanding of proton transfer phenomenon at the molecular level has become a fundamental problem in many areas of science, from biological systems[1,2] to electrochemical devices.[3,4] Although a large portion of activities in the fields of molecular biology and pharmacology was dedicated to recognizing the biological consequences of intramolecular protonic charge diffusion in drugs and nucleic acids,[5−7] the effect of intermolecular proton transport on the physicochemical properties of ion-containing systems has attracted enormous attention of chemists and material scientists.[8,9] Following the latter research strategy, it has been demonstrated that proton conductors are promising electrolytes in fuel cells and batteries.[10] Unfortunately, most of these systems are water-saturated materials characterized by relatively poor proton conductivity in anhydrous conditions that limits their commercial application. To date, there are only few examples of dry superprotonic glasses and polymers.[11−14] Therefore, one of the key challenges in advancing the electrochemical technology lies in new protic ionic liquids and solids characterized by long-term thermal stability and high electric conductivity at low relative humidity. To address these issues, there is a need to understand the molecular mechanism of enhanced proton transport in anhydrous ionic systems.

From a fundamental point of view, two types of charge transport mechanisms have been recognized for proton conductors. In the case of so-called vehicular mechanism, the charge transfer is associated with the motions of entire ions. A key feature of the other, frequently referred to as the Grotthuss type, is the local proton hopping through the H-bond network.[15] As our knowledge has advanced, it has been found that the Grotthuss picture, originally proposed to explain the enhanced proton conductivity in water,[16] might decouple proton transport from the mass diffusion. It means that the conducting units (protons) become more mobile than the species controlling the structural relaxation. This is in contrast with the vehicle mechanism in which all species move at a similar rate.

It has been demonstrated that the most efficient experimental method to examine the degree of coupling and decoupling of different molecular motions and consequently to identify the conductivity mechanism in ionic and nonionic systems is dielectric spectroscopy.[17−19] In this type of measurements, the specific separation between the time scale of charge and mass diffusion is manifested by a well-defined break of the temperature dependence of dc

conductivity (σdc ) or conductivity relaxation times (τσ ), from the Vogel− Fulcher− Tammann-like (T > Tg ) to Arrhenius behaviour (T < Tg ), observed at τσ much shorter than 102 s. Nevertheless, the greatest advantage of this method is an unusual opportunity to investigate the σdc and τσ behaviour at elevated pressure, both at isobaric and isothermal conditions. Interestingly, it has been demonstrated that compression markedly enhances the decoupling of charge transfer from the structural relaxation when conductivity of ionic system is governed by fast proton hopping in accordance with the Grotthuss-mechanism.[17,20,21] This finding indicates that, in contrast to ambient conditions, at elevated pressure when the H-bonded network is strongly reinforced the proton transport is much more efficient.

The dielectric experiments performed so far clearly indicate that the Grotthuss-type transport, reflected in the anomalous electrical conductivity behaviour dc(T,P) , gives rise to superprotonic properties of phosphoric acid,[22] hydrated acidic polymers,[23] and non-ionic azole membranes[24] as well as some anhydrous organic protic salt systems formed via neutralization of a Brønsted acid with a corresponding base.[13,25,26] Surprisingly, in the case of conventional imidazolium-based protic ionic liquids (ILs) the charge transfer is mostly coupled to structural relaxation.[14,27] The reason lies in the complete ionization of these systems combined with a low value of self-dissociation coefficient of the cation with both nitrogen atoms protonated. Therefore, there is a growing interest to design new anhydrous salts with a chemical structure providing exceptionally high proton conductivity.

In this study, we examine the proton transfer mechanism in seven newly synthesized protic ionic salts based on the same cation, lidocaine, and various organic and inorganic anions containing different number of proton-active sites and characterized by different proton donor/acceptor capability. The systems of interest, having various ionization degrees, enable us to provide a resolution to the long-standing question of factors controlling the enhanced proton conductivity in anhydrous ionic materials. To address this issue, we investigate the interplay between the charge transport and structural dynamics by means of isothermal and isobaric dielectric measurements as well as various calorimetric methods. Additionally, to describe the possible pathways of mobility of the charge carrier the experimental data were accompanied by DFT calculations.

## Materials and Methods

### Examined Ionic Conductors

In this paper, we have examined the proton transfer ability of seven newly synthesized lidocaine based systems. A detailed synthesis protocol is described in Supporting Information. Among the studied systems lidocaine docusate and lidocaine hydrogen citrate are liquid at room condition while the other salts take the form of white, crystalline powders with the melting points summarized in Table 1. To investigate the ions transport properties of lidocaine salts the crystalline samples were converted to the amorphous form by means of simple vitrification technique. The water content of the examined ILs was determined by Karl Fischer titration and it was lower than 60 ppm, that is, 0.006 wt %.

### Dielectric Measurements

The dielectric spectra of examined samples were measured using a Novocontrol Alpha Analyzer Concept 80. The measurements were conducted in a stainless-steel electrodes (diameter = 20 mm) capacitor with a gap of 0.1 mm. The high-pressure experiments were performed in a Unipress system with a custom flat parallel capacitor. A detailed description of the high-pressure equipment can be found in ref.[28].

### Calorimetric Measurements

The frequency dependency of the calorimetric glass transition temperature was measured by temperature modulated differential scanning calorimetry (TMDSC) employing a PerkinElmer Pyris Diamond DSC (1.6Å~ 10−3 Hz < f < 0.1 Hz) and a Mettler Toledo Flash DSC 1(0.3 Hz < f < 50 Hz). A step response multi frequency data analysis was applied.[29] For the highest frequencies (40 Hz < f <13 kHz) a chip based AC calorimeter was used.30 All measurements were performed in a dry nitrogen atmosphere and the samples were dried in the instruments prior to the measurements.

### Simulation Details

All calculations were performed using the ORCA 3.02 quantum chemistry package.31 Most of the calculations were done applying density functional theory (DFT) with B3LYP hybrid functional and D3 dispersion corrections. Initial geometry scans were performed in 6-31G* basis set, whereas stationary point geometry optimizations were performed in 6-311G* basis set. In order to verify correctness of stationary states (minima and saddle point),

vibrational analysis was performed. Moreover, to verify the DFT method, which sometimes enhances charge delocalization of the system, RI-MP2 method with the use of cc-pvdz basis set was employed.

**Results**

General.

The examined herein ionic compounds were designed as model systems to understand the molecular mechanism of charge transport in anhydrous protic conductors. As such, a lidocaine base (L), one of the most popular anesthetic agent, has been selected as the major component of the studied series. There are at least two fundamental reasons to justify this selection. Firstly, in X-ray investigations combined with the recent dielectric studies of lidocaine hydrochloride salt,[21] it was argued that lidocaine cations tend to link to each other forming strongly hydrogen bonded chains,[32] an excellent network for fast proton hopping. Secondly, we have found that under appropriate conditions the lidocaine molecule is able to undergo an intramolecular proton transfer reaction and consequently to exist as a mixture of two easily interconvertible constitutional isomers. Thus, one can expect that the unique chemical structure of lidocaine has a potential to favor the proton hopping in ionic systems. To shed more light on this, we have chosen seven different acids to create Brønsted pairs with lidocaine base. Some physicochemical properties of the newly synthesized salts are briefly listed in Table 1.

The initial thermal characterization of the studied systems has shown that these lidocaine salts are good glass formers, that is, they do not have a tendency to form an ordered structure from the amorphous state. The only exception is the hemisulfate salt with a crystallization onset detected above 376 K. Nevertheless, this ionic conductor appears to be the most promising among the series of lidocaine salts produced. This is due to the sulfonate groups that are frequently regarded as a source of high proton conductivity of polymer electrolyte membranes.[34] Likewise, of a great importance is the dihydrogen phosphate salt due to the highly efficient Grotthuss mechanism confirmed in phosphoric acid.[22] On the other hand, the hemisuccinate, hydrogen citrate, and acetate salts were prepared to further advance our understanding of the relationships between the number of proton-active sites and ion transport properties of anhydrous protic conductors. This is in contrast with hydrobromide and docusate systems that are characterized by the smallest and the largest anion, respectively, among the produced salts.

Dielectric and Calorimetric Data.

To examine the charge transport mechanism of lidocaine-based ionic conductors, dielectric measurements over a wide frequency, temperature and pressure range were performed. Following the standard practice, the complex electrical modulus representation $M^*(f) = M'(f) + iM''(f)$ has been adopted to analyze the experimental data.[35−37] Herein, it should be noted that physically the electric modulus corresponds to the relaxation of the electric field in the material when the electric displacement remains constant. Consequently, the $M^*$ formalism represents the real dielectric relaxation process. This representation allows determination of two relevant quantities describing the ion dynamics in conducting materials, that is, the dc conductivity calculated from $M''$ in the low-frequency region, $\sigma_{dc} \approx 2\pi f \varepsilon_0 / M''$, and the conductivity relaxation time estimated from the frequency corresponding to the $M''$ maximum, $\tau_\sigma = 1/2\pi f_{max}$. The representative modulus loss spectra $M''(f)$ of lidocaine hemisuccinate collected over a wide temperature range at ambient pressure conditions are depicted in the upper inset of Figure 1.

As demonstrated, the maximum of the prominent $M''$ peak, related to the translational mobility of ions, moves toward lower frequencies with cooling. However, below a certain temperature this effect is markedly reduced. Concomitantly, at the same temperature where the spectra are getting closer the $\tau_\sigma(T)$ dependence reveals a well-defined break from the Vogel− Fulcher− Tammann− like to Arrhenius behavior (Figure 1). According to the latest reports on protic ionic conductors, the observed crossover is a manifestation of the liquid−glass transition of the ionic glass former.[13,17,20] In this context, it is crucial to note that the glass transition (Tg) is usually defined as the temperature at which the structural relaxation time ($\tau_\alpha$) reaches 1000 s.[36] However, for the hemisuccinate salt the conductivity relaxation time at the Tg point is even 100-fold faster than $\tau_\alpha$, $\tau_\sigma \sim 5$ s. This result suggests that in this case of the protic conductor there is a distinctive separation (decoupling) between the time-scale of ionic transport and structural relaxation in the vicinity of the glass transition temperature, that is, the charge transfer is continued when the host dynamics became arrested. Nevertheless, to investigate this phenomenon in more detail it is necessary to obtain information on the temperature behavior of structural relaxation times of the studied ionic materials. Herein, the $\tau_\alpha(T)$ dependences were determined by means of various calorimetric techniques (details are presented in Supporting Information). As illustrated in Figure 1, from comparison of $\tau_\sigma(T)$ data of lidocaine hemisuccinate and its temperature dependence of $\tau_\alpha$ determined over a six-decades range, it is obvious that the abrupt inflection of the conductivity relaxation curve

occurs at log($\tau_\alpha$ /s ) = 3. As a consequence, the ions movement through the studied system is indeed decoupled from the structural dynamics. Furthermore, the application of pressure (P) as an external thermodynamic variable markedly enhances the decoupling between $\tau_\sigma$ and $\tau_\alpha$ in the hemisuccinate salt, that is, the kink of the isothermal $\tau_\sigma$ (P) curve being a manifestation of glass transition pressure, Pg moves toward shorter conductivity relaxation times as pressure increases. This is clearly visible in the lower inset panel of Figure 1. Because the crossover bending points on the $\tau_\sigma$ – P plot denote the Tg (Pg) line, one can easily estimate the dTg /dP|P=0.1MPa coefficient that reflects the pressure sensitivity of the glass transition temperature for the examined ionic conductor. Interestingly, the small value of dTg /dP = 0.127 K/MPa for lidocaine hemisuccinate, much lower than those found for other protic ionic conductors,[17,39] reflects a weak compressibility of the sample probably caused by strongly hydrogen-bonded structure.

The next step of our investigations was dedicated to dielectric and calorimetric studies of other lidocaine-based ionic compounds. From Figure 2, it becomes clear that the greatest separation between the time scale of conductivity and structural relaxation occurs near Tg of lidocaine di(dihydrogen phosphate). Surprisingly, in this system the charge diffusion is even faster than that found in the classical protonic conductor, $H_3PO_4$ acid.

Ranking the various lidocaine salts in terms of the decoupling force, the dihydrogen citrate salt takes the second place. On the other hand, a less pronounced difference between the ions translation and host molecule reorientation is observed for inorganic lidocaine salts, that is, hydrobromide and hemisulfate. These results stand in sharp contrast with the behavior of lidocaine acetate and docusate, where the ionic conductivity was found to be completely coupled to structural relaxation. Interestingly, even compressing the sample up to 400 MPa was not able to separate $\tau_\alpha$ and $\tau_\sigma$ (see Figure 3).

**Discussion**

Internal Proton Transfer within the Lidocaine Cation.

A varying degree of decoupling between charge diffusion and structural dynamics was observed when we applied the same experimental protocol to a series of protic compounds, based on one active pharmaceutical ingredient, lidocaine. It means that the chemical structure of the anion has a particularly strong influence on the charge transport properties of lidocaine salts. To provide the physical insight into this issue, theoretical calculation studies were performed. Because all the examined samples were formed by proton transfer reaction between

Brønsted acids and bases, at the beginning, we considered the reversed reaction, that is, simple proton dissociation from the lidocaine cation (Figure 4, conversions A−E).

The energy needed for the standard proton detachment evaluated by DFT falls within the range of 60−80 kJ/mol. However, we have found that a much lower activation barrier is required for proton hopping from the nitrogen (R3NH +) to the oxygen atom of the carbonyl group (R2C  O) (pathways A−B in Figure 4). Such an intramolecular proton migration implicates the rearrangement of chemical bonds in the lidocaine molecule, the charge displacement and finally the hydrogen dissociation from the R2NH+ group. This ionic tautomerization, markedly different than the classical amide-imidic acid conversion (schemes A− B), requires only 10− 15 kJ/mol and thus facilitates the charge diffusion through the system. However, only some of the examined anions appeared to work as efficient proton-relay molecules. Consequently, the fast proton conduction is a characteristic feature of some studied herein systems.

Proton Transfer Mechanism in Anhydrous Lidocaine Salts.

We have found that among the chosen salts, the docusate structure sterically blocks the proton hopping, whereas the acetate anion readily accepts proton and acquires the form of energetically preferred neutral acetic acid. This is due to the poor donor capability of acetate anion as well as relatively low value of Δ pKa for lidocaine acetate. As a consequence, at ambient and elevated pressure conditions the conductivity of these two ionic systems is governed by translational diffusion of large molecular species and therefore $\tau_\alpha$ and $\tau_\sigma$ are fully coupled. Considerably different conductivity trace occurs in the case of hemisuccinate salt that is characterized by Δ pKa similar to that established for L-acetate (see Table 1). The hydroxyl moieties actively involved in charge transfer combined with passable donor capability of anion and an extensive H-bonded network (see Figure S9 and Table S1 in Supporting Information) make the succinate structure an effective proton mediator. The representative proton migration pathway through the hemisuccinate ion, imposed by the external electric field, is visualized in Figure 5.

It can be easily seen that the examined anion, due to the dual proton active site, is able to act as a bridge between two neighboring lidocaine molecules: (i) the charged imidic-acid structure, being a consequence of internal tautomerization reaction and (ii) the neutral form existing in the system due to its incomplete ionization. These theoretical considerations were confirmed by experimental results, showing the decoupling between conductivity and structural relaxation times for lidocaine hemisuccinate in contrast to simple VFT behaviour of

τσ (T) reported in the case of acetate and docusate salts. Additionally, the separation between the time scale of charge and mass diffusion in the succinate system becomes even greater under high pressure conditions. These findings indicate that compression not only reduces intermolecular distances but also markedly affects the H-bonded structure of compressed material and, thus, creates new pathways for fast proton hopping. In the light of these theoretical considerations supported by experimental data, one can state that at least two proton active moieties in the anion are required to enhance the Grotthuss conduction through the lidocaine systems. However, the more proton donors in chemical structure, the more efficient charge transfer is expected. Therefore, the dihydrogen citrate, dihydrogen phosphate, and hemisulfate anions are potentially better proton-relay molecules than the hemisuccinate form. However, as presented in Figure 2, the decoupling between the charge migration and structural relaxation at Tg is larger than that observed for hemisuccinate salt only in the case of dihydrogen citrate (3 decades) and phosphate (7 decades) systems. On the other hand, the time scale separation between τσ and τα is less pronounced in lidocaine hemisulfate. This apparently surprising result can be very easy explained if we take into account the ionization degree of this protic conductor. Namely, hemisulfate salts, just like L-hydrochloride and L-hydrobromide and in contrast to other examined herein lidocaine-based compounds, is composed solely of ions (Δ pKa > 13). However, according to the literature reports the ability of ionic system to fast proton conduction is strongly governed by nonconducting species that fulfil the role of extra H+ -donor/acceptor.[40,41] That is why in the sulfate salt (as well as in L-HBr) the Grotthuss mechanism is less effective than the charge diffusion in succinate system. As a consequence the decoupling index observed in L-sulfate is smaller than that calculated for L-hemisuccinate, despite the higher number of proton active sites in $H2\ SO4^-$ anion. Note that the proton transfer is still realized through the H-bonds connecting R2 N+ -H groups and acid sulfate anions, but importantly, there is no affinity of system to deionization. Interestingly, the most efficient Grotthuss conduction among the systems studied herein is observed in the case of lidocaine di(dihydrogen phosphate). This is due to the doubly ionized lidocaine structure (form F in Figure 4) combined with the increased amount of anionic charge carriers that are characterized by a high proton donor/acceptor capability. Moreover, it should be stressed that the analysis of the Ldi (dihydrogen phosphate) crystal structure has shown that this protic ionic compound is characterized by an extensive H-bonded network that is crucial in the Grotthuss-type transport mechanism (see Figure S10 and Table S1 in Supporting Information). Moreover, we have found that the amide group is assisted on both sides by two possibly partially deprotonated phosphate molecules. This arrangement may play an important role in a transfer

of proton charge through delocalized covalent bonds of the amide moiety during the tautomerization process. Moreover, phosphate molecules on their own from a crown-like layered, self-assembled arrangement which looks like a promising route of proton transfer with possibly a lower activation energy due to already partial deprotonation and strong dislocation of protons (see Figure 6).

Conductivity Behavior of Examined Systems.

Considering the molecular origin of enhanced proton conduction it is also necessary to explore the temperature dependence of electrical conductivity σdc for the studied herein ionic conductors. As summarized in Figure 7, the ionic conductivity of docusate and acetate lidocaine salts is 10−15 S/cm at Tg , which is in a good agreement with the literature statements on the ideally coupled ionic glasses. However, with the increased number of proton active sites in the chemical structure of anion the σdc (Tg) is also raised.

In the case of lidocaine di(dihydrogen phosphate), the difference is ~ 7 orders of magnitude. This indicates that the excess proton conductivity is revealed not only in the decoupling phenomenon but also gives a real contribution to the value of electrical conductivity of ionic systems. Furthermore, due to the Grotthuss-type mechanism, σdc of glasses being a mixture of ions and neutral species (like the hemisuccinate salt) is even higher than that found for completely ionized salts (e.g., lidocaine HBr; see the data in Table 1).

Taking these facts together one can state that the examined herein dihydrogen phosphate, dihydrogen citrate, and hemisuccinate lidocaine salts can be classified as new examples of anhydrous superprotonic conductors for potential fuel cell applications. However, as indicated by our experimental data the most promising is phosphate-based material. Interestingly, among the dry proton conductors identified so far, mostly phosphate salts can be found (e.g., carvedilol dihydrogen phosphate or trimethylammonium dihydrogen phosphate). Thus, when designing an anhydrous materials with exceptionally high proton conductivity, the phosphate anion is of particular interest. On the other hand, it is better to avoid: (i) a large anions that sterically blocks the proton transfer; (ii) anions with only one proton active sites and poor proton donor/acceptor capability; (iii) sulfate groups that seems to be a source of high proton conductivity only in the case of polymer electrolyte membranes because the dc-conductivity of these systems is realized mainly by the vehicular mechanism.

**Summary**

We conclude this article by highlighting the factors controlling the enhanced proton conductivity in anhydrous ionic materials. As demonstrated by theoretical and experimental data, systems characterized by an internal charge transfer reaction are potential proton conductors for various electrochemical applications. This is because the tautomerization process markedly reduces the energy required for fast proton hopping between the ions and neutral species. However, based on the dielectric studies of various lidocaine salts supported by DFT calculations we have shown that regarding the ability of given system to fast proton conduction the ionization degree should be also discussed. Δ pKa value must be high enough to meet the criteria of ionic liquid; however, at the same time, it cannot be too exaggerated since a nonconductive species fulfil the role of efficient H+ -carriers. Considering the molecular origin of fast proton transport in ionic systems one should also take into account the characteristics of H-bond network in examined material, the number of active sites in the chemical structure of ions as well as their proton donor/acceptor capability. This is because all these factors together significantly facilitate the Grotthuss mechanism by creating a shortcut for charge transport and consequently cause a relatively large separation between the time scale of charge and mass diffusion that is observed experimentally as a characteristic crossover of $\tau\sigma$ (T) dependence.

**Acknowledgements**

M.P., Z.W., S.H.B. are deeply grateful for the financial support by the National Science Centre within the framework of the Opus project (Grant No. DEC 2011/03/B/ST3/02072). K.G. and P.W. are deeply grateful for the financial support by the National Science Centre within the framework of the Opus3 project (Grant No. DEC-2012/05/B/ST3/02837). Z.W. acknowledges the financial assistance from FNP START (2014). E.S. acknowledges financial support from the Interdisciplinary Faculty, University of Rostock. L.T. acknowledges the financial support from the Science Foundation Ireland under grant No. 12/RC/2275 (Synthesis and Solid State Pharmaceuticals Centre).

**References**

(1) Kreuer, K. D. Chem. Mater. 1996, 8, 610−641.

(2) Yvonne, M. J. Comput.-Aided Mol. Des. 2010, 24 (6−7), 473−474.

(3) Armand, M.; Endres, F.; MacFarlane, D. R.; Ohno, H.; Scrosati, B. Nat. Mater. 2009, 8, 621−629.

(4) Belieres, J. P.; Gervasio, D.; Angell, C. A. Chem. Commun. 2006, 0, 4799−4801 DOI: 10.1039/B611150E.

(5) Paneth, P. Kinetics and Dynamics: From Nano- to Bio-Scale; Springer: New York, 2010.

(6) Wojnarowska, Z.; Wlodarczyk, P.; Kaminski, K.; Grzybowska, K.; Hawelek, L.; Paluch, M. J. Chem. Phys. 2010, 133, 094507.

(7) Wojnarowska, Z.; Paluch, M.; Wlodarczyk, P.; Dulski, M.; Wrzalik, R.; Roland, C. M. J. Phys. Chem. Lett. 2012, 3 (16), 2288−2292.

(8) MacFarlane, D. R.; Forsyth, M.; Izgorodina, E. I.; Abbott, A. P.; Annat, G.; Fraser, K. Phys. Chem. Chem. Phys. 2009, 11, 4962.

(9) Gourdoupi, N.; Kallitsis, J. K.; Neophytides, S. J. Power Sources 2010, 195, 170−174.

(10) Bennett, M. D.; Leo, D. J.; Wilkes, G. L.; Bayer, F. L.; Pechar, T. W. Polymer 2006, 47, 6782−6796.

(11) Einsla, M. L.; Kim, J. S.; Hawley, M.; Lee, H. S.; McGrath, J. E.; Liu, B.; Guiver, M. D.; Pivovar, B. S. Chem. Mater. 2007, 20, 5636−5642.

(12) Kim, S. Y.; Kim, S.; Park, M. J. Nat. Commun. 2010, 1, 88.

(13) Mizuno, F.; Belieres, J. P.; Kuwata, N.; Pradel, A.; Ribes, M.; Angell, C. A. J. Non-Cryst. Solids 2006, 352, 5147−5155.

(14) Kreuer, K. D.; Paddison, S. J.; Spohr, E.; Schuster, M. Chem. Rev. 2004, 104, 4637−4678.

(15) Agmon, N. Chem. Phys. Lett. 1995, 244, 456−462.

(16) Marx, D. ChemPhysChem. 2006, 7, 1848−1870.

(17) Wojnarowska, Z.; Wang, Y.; Pionteck, J.; Grzybowska, K.; Sokolov, A. P.; Paluch, M. Phys. Rev. Lett. 2013, 111 (22), 225703.

(18) Wojnarowska, Z.; Knapik, J.; Díaz, M.; Ortiz, A.; Ortiz, I.; Paluch, M. Macromolecules 2014, 47 (12), 4056−4065.

(19) Wang, Y.; Lane, N. A.; Sun, C. N.; Fan, F.; Zawodzinski, T. A.; Sokolov, A. P. J. Phys. Chem. B 2013, 117, 8003−8009 DOI: 10.1021/jp403867a.

(20) Wojnarowska, Z.; Roland, C. M.; Swiety-Pospiech, A.; Grzybowska, K.; Paluch, M. Phys. Rev. Lett. 2012, 108, 015701.

(21) Swiety-Pospiech, A.; Wojnarowska, Z.; Hensel-Bielowka, S.; Pionteck, J.; Paluch, M. J. Chem. Phys. 2013, 138 (20), 204502.
(22) Vilčiauskas, L.; Tuckerman, M. E.; Bester, G.; Paddison, S. J.; Kreuer, K. D. Nat. Chem. 2012, 4, 461−466.
(23) Knauth, P.; Di Vona, M. L. ECS Meeting Abstracts; The Electrochemical Society: Pennington, NJ, 2012; Vol. 02, issue 13, pp 1353.
(24) Choi, P.; Jalani, N. H.; Datta, R. J. Electrochem. Soc. 2005, 152, E123−E130.
(25) Wojnarowska, Z.; Roland, C. M.; Kolodziejczyk, K.; Swiety-Pospiech, A.; Grzybowska, K.; Paluch, M. J. Phys. Chem. Lett. 2012, 3, 1238.
(26) Wojnarowska, Z.; Wang, Y.; Paluch, K. J.; Sokolov, A. P.; Paluch, M. Phys. Chem. Chem. Phys. 2014, 16, 9123.
(27) Thawarkar, S.; Khupse, N. D.; Kumar, A. Phys. Chem. Chem. Phys. 2014, DOI: 10.1039/c4cp04591b.
(28) Roland, C. M.; Hensel-Bielowka, S.; Paluch, M.; Casalini, R. Rep. Prog. Phys. 2005, 68, 1405.
(29) Shoifet, E.; Schulz, G.; Schick, C. Thermochim. Acta 2014, No. http://dx.doi.org/10.1016/j.tca.2014.10.010.
(30) Huth, H.; Minakov, A.; Schick, C. Netsu Sokutei 2005, 32 (2), 70−76.
(31) Neese, F. Wiley Interdiscip. Rev.: Comput. Mol. Sci. 2012, 2, 73− 78 DOI: 10.1002/wcms.81.
(32) Hanson, A. W.; Rohlh, M. Acta Crystallogr., Sect. B: Struct. Crystallogr. Cryst. Chem. 1972, 28, 3567.
(33) Wojnarowska, Z.; Grzybowska, K.; Hawelek, L.; Swiety- Pospiech, A.; Masiewicz, E.; Paluch, M.; Sawicki, W.; Chmielewska,
A.; Bujak, P.; Markowski, J. Mol. Pharmaceutics 2012, 9 (5), 1250− 1261.
(34) Higashihara, T.; Matsumoto, K.; Ueda, M. Polymer 2009, 97, 5341−5357.
(35) Howell, F. S.; Bose, R. A.; Macedo, P. B.; Moynihan, C. T. J. Phys. Chem. 1974, 78, 639−648.
(36) Kremer, F.; Schoenhals, A. Broadband Dielectric Spectroscopy; Kremer, F., Schoenhals, Eds.; Springer-Verlag: Berlin, 2003; pp 1−32.
(37) Hodge, I. M.; Ngai, K. L.; Moynihan, C. T. J. Non-Cryst. Solids 2005, 351, 104.
(38) Floudas, G.; Paluch, M.; Grzybowski, A.; Ngai, K. L. Molecular Dynamics of Glass-Forming Systems: Effects of Pressure; Eds.; Springer- Verlag: Berlin, 2011; pp 1−34.

(39) Wojnarowska, Z.; Paluch, M.; Grzybowski, A.; Adrjanowicz, K.; Grzybowska, K.; Kaminski, K.; Wlodarczyk, P.; Pionteck, J. J. Chem. Phys. 2009, 131, 104505.
(40) Hoarfrost, M. L.; Tyagi, M.; Segalman, R. A.; Reimer, J. A. J. Phys. Chem. B 2012, 116 (28), 8201−9.
(41) Noda, A.; Susan, M. A. B. H.; Kudo, K.; Mitsushima, S.; Hayamizu, K.; Watanabe, M. J. Phys. Chem. B 2003, 107, 4024.

**Figures**

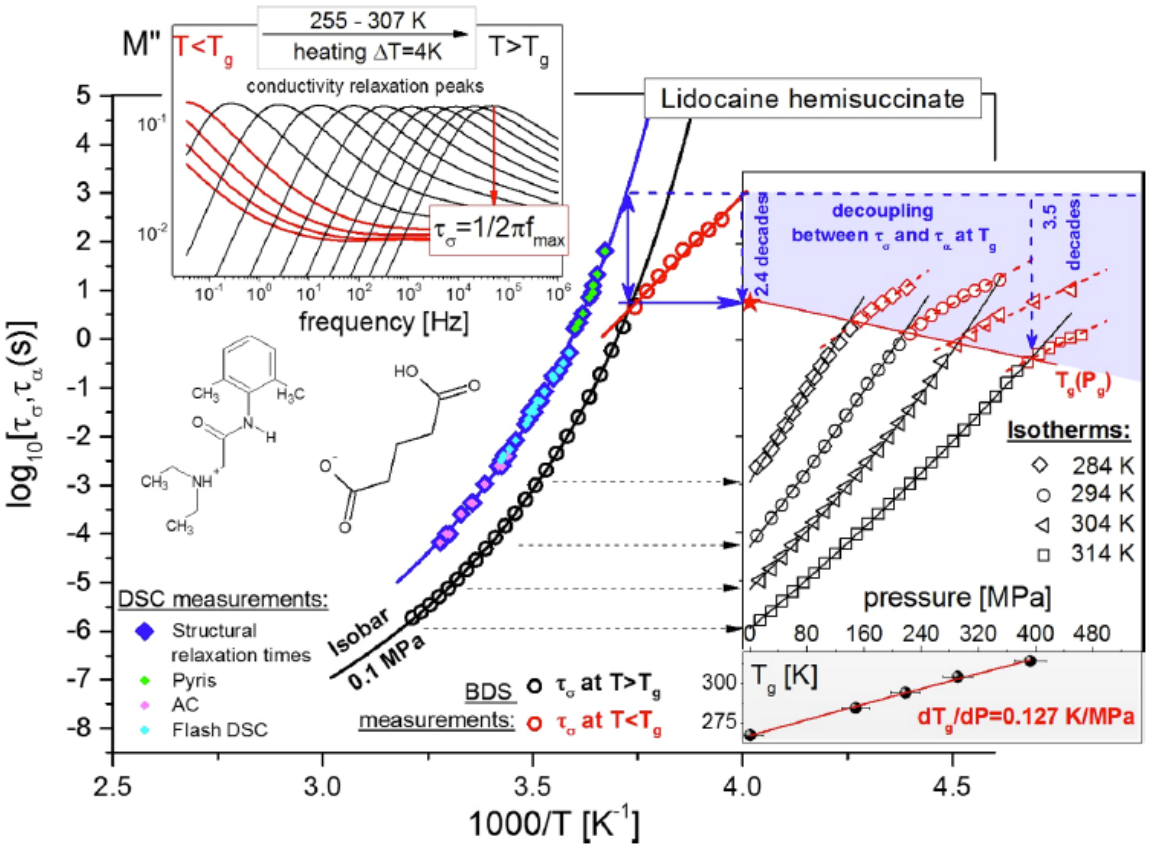


Figure 1. Main panel: the temperature dependence of conductivity relaxation time recorded by means of dielectric spectroscopy at ambient pressure both above (black circles) and below Tg (red circles); the structural relaxation times as a function of 1/T (blue diamonds) determined from the various calorimetric techniques. Inset panel (upper): dielectric loss modulus spectra due to conductivity relaxation at various temperatures in the liquid and glassy states for lidocaine hemisuccinate. Inset panel (lower): isothermal dielectric measurements of conductivity relaxation time of lidocaine hemisuccinate; the pressure dependence of Tg for this compound. The temperature dependence of τσ above Tg were parametrized by the VFT equation: $\tau\sigma = \tau\sigma 0\exp[B/(T - T0)]$, whereas τσ(P) curves were described by the pressure counterpart of VFT law $\tau\sigma = \tau\sigma 0\exp[BP/(P - P0)]$.38

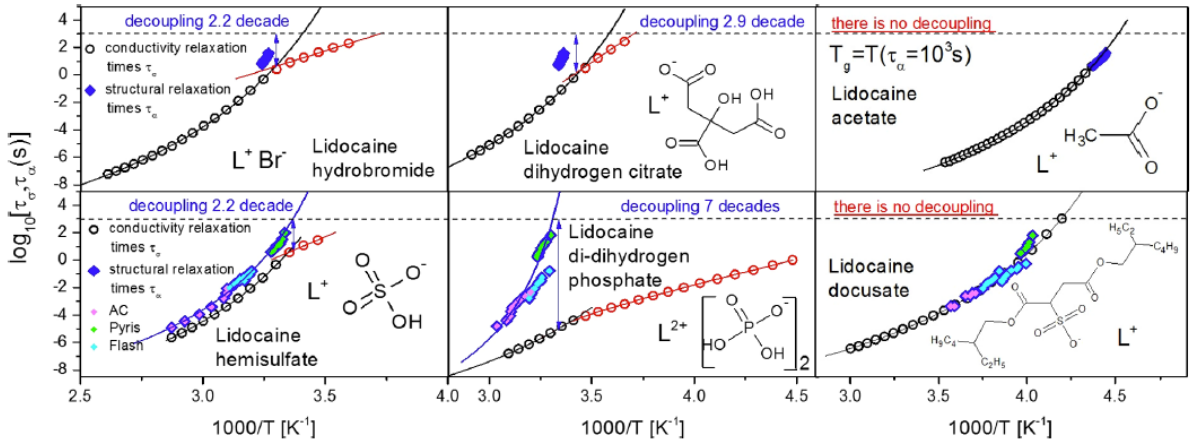


Figure 2. Temperature dependences of conductivity and structural relaxation times for six different lidocaine-based systems.

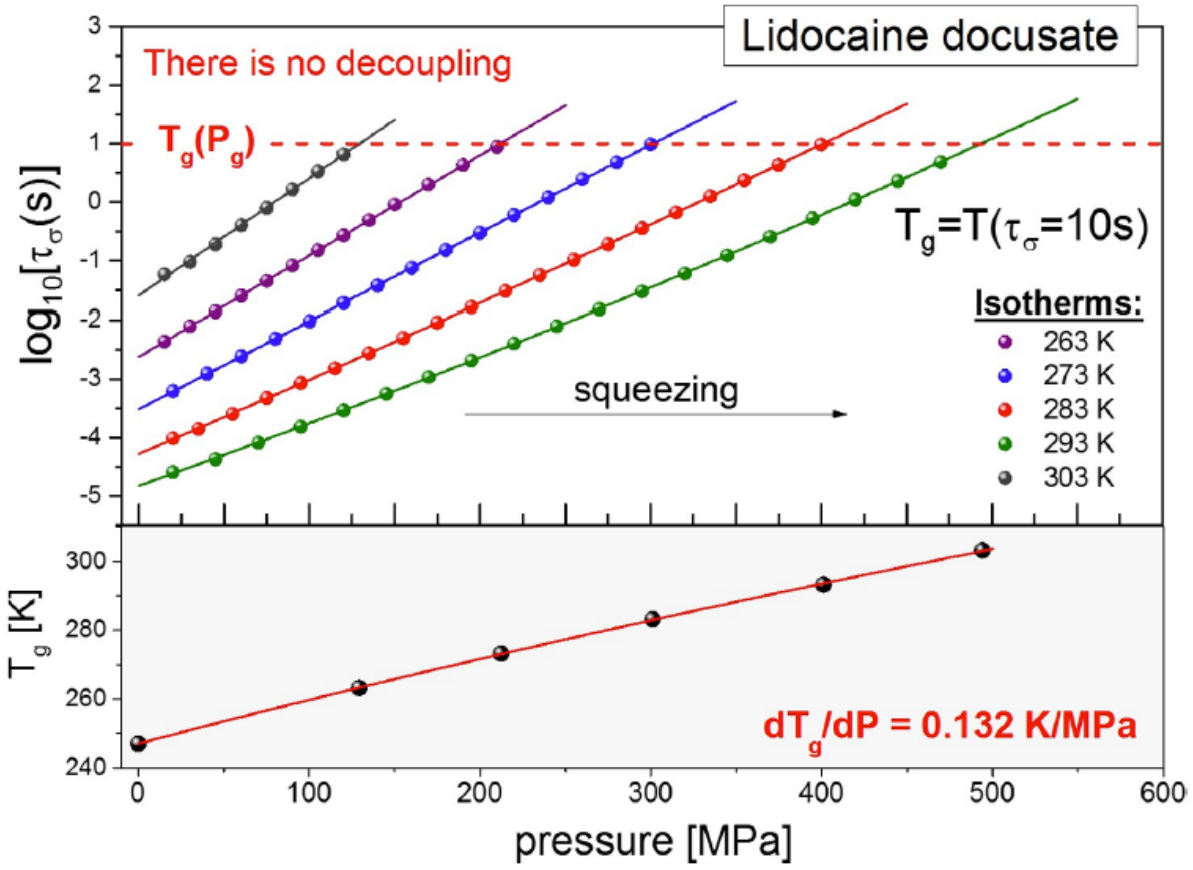


Figure 3. Isothermal dielectric measurements of conductivity relaxation time of lidocaine docusate. Solid lines denote fits of VFTp equation to the experimental data.

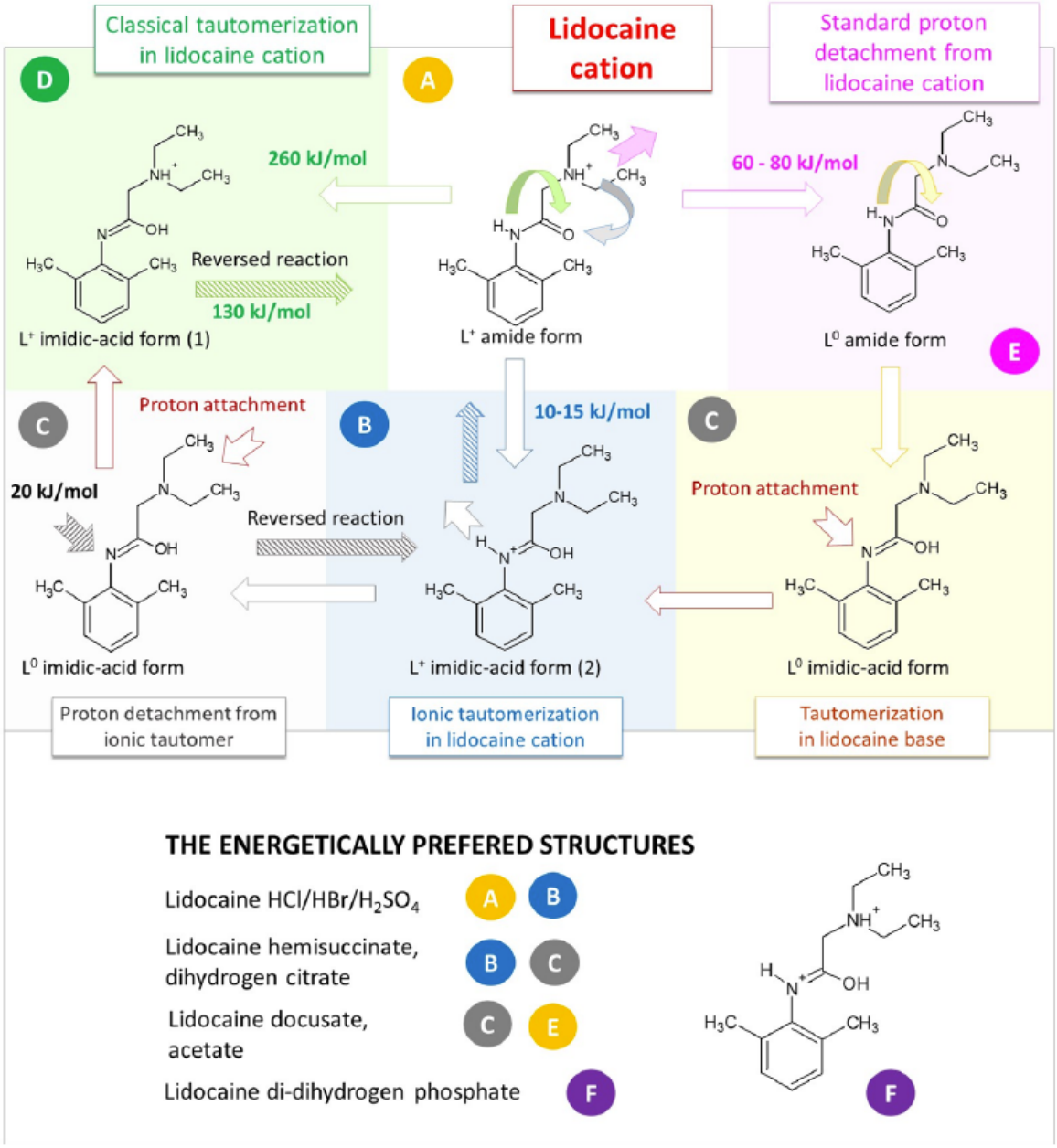


Figure 4. Possible pathways for proton transfer within the lidocaine structure.

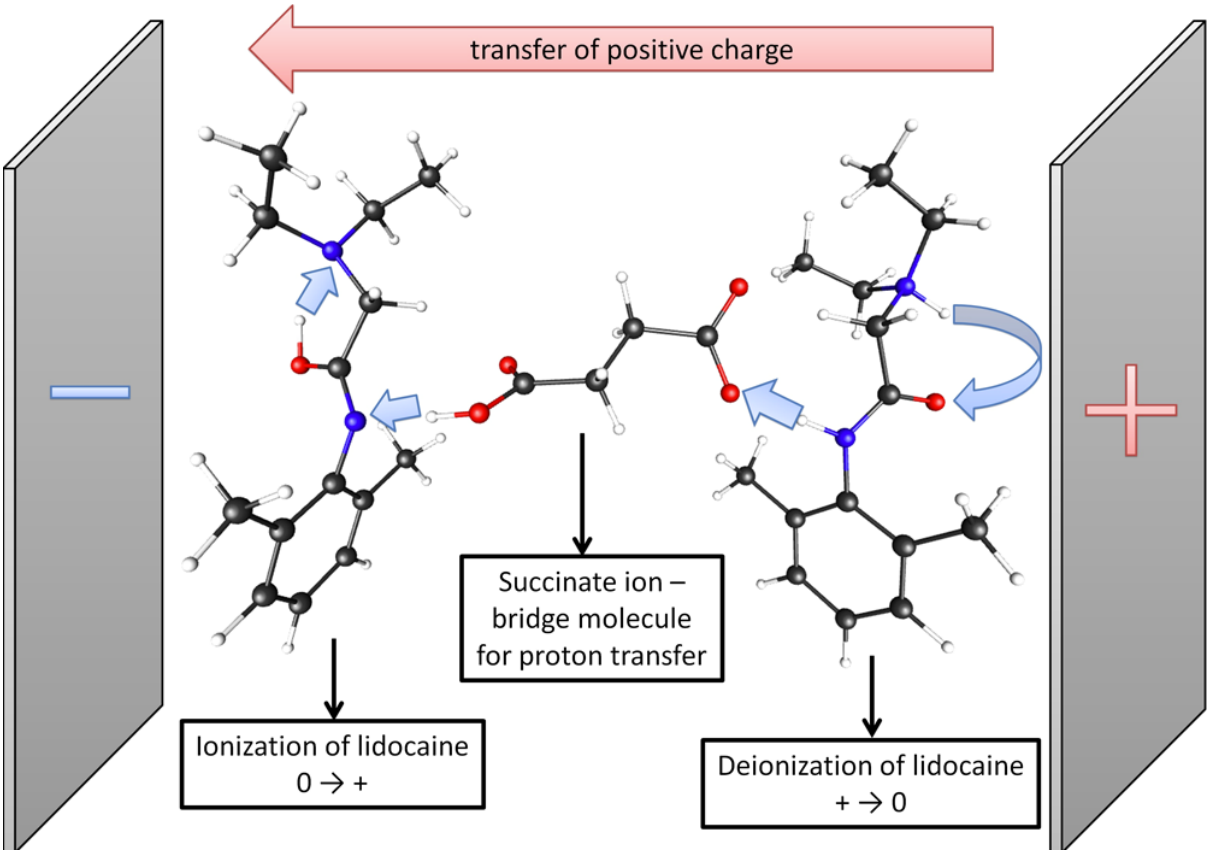


Figure 5. Representative proton migration pathway through the hemisuccinate anion imposed by the external electric field. The arrows on the right side of the figure indicate the internal proton transfer reaction within the lidocaine structure (A−B stage in Figure 4) and the proton detachment from R2NH + group (B−C in Figure 4), respectively. On the other hand, the arrows on the left part of figure indicate the proton transfer between anion and L-molecule (C−B stage in Figure 4) and the proton hopping in lidocaine cation (B−A stage in Figure 4).

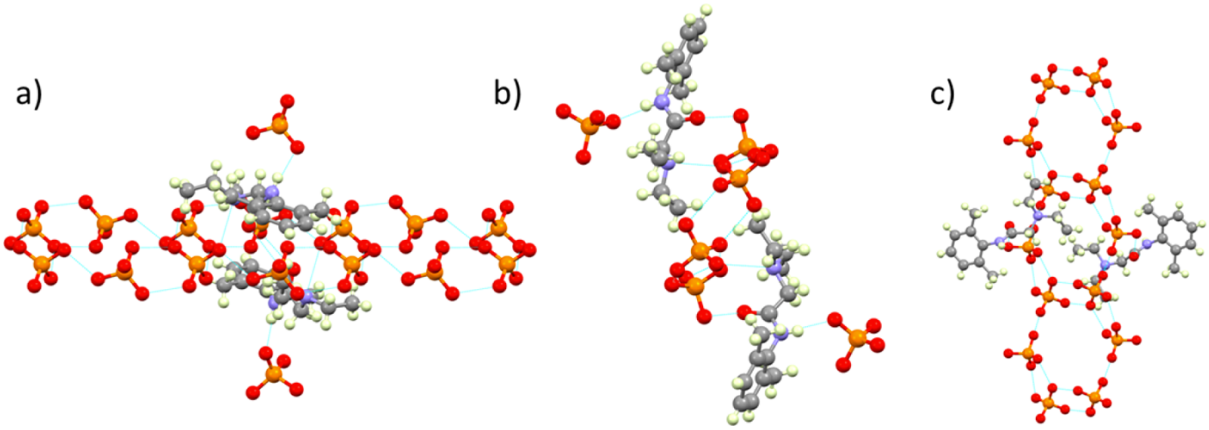


Figure 6. Crown cluster motifs of phosphate molecules along: (a) a axis, (b) b axis, and (c) c axis with exemplar amide “bridges” of lidocaine molecules. Some molecules of lidocaine were removed for clarity purposes.

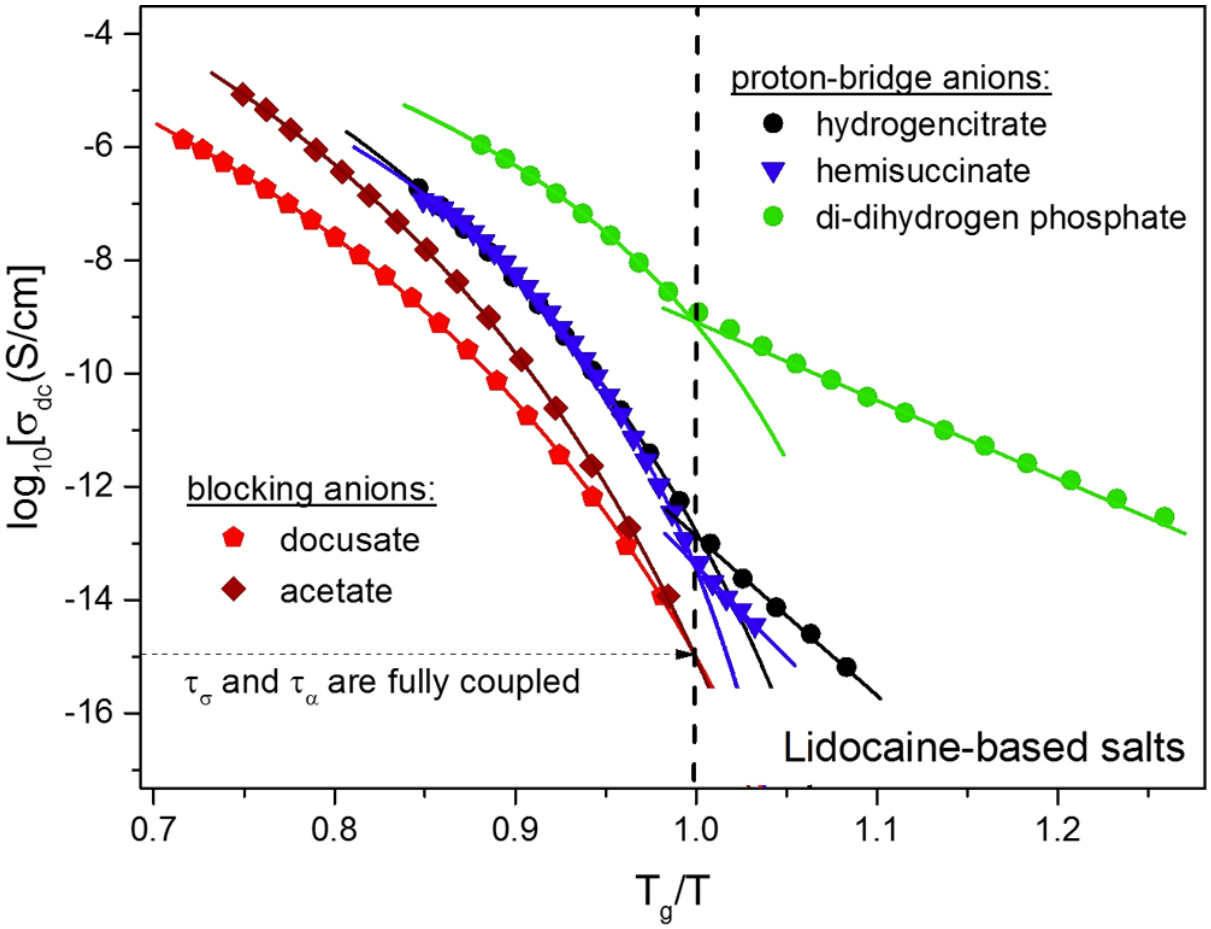


Figure 7. Tg-scaled Arrhenius plot for the conductivities of examined ionic glasses.

**Tables**

Table 1. Characteristics of Protic Ionic Conductors Used in This Study

| protic ionic salts used | Tg [K] ΔpKa | $\Delta C_P$ [J g/K] | $T_m$ [K] | $\Delta H_m$ [J/g] | $T_c$ [K] | $\Delta H_c$ [J/g] | $\Delta pK_a$ | $\sigma_{dc}(Tg)$ [S/cm] |
|---|---|---|---|---|---|---|---|---|
| L-HCl | 307 | 0.41 | 343 | | | | 13.96 | $5.02 \times 10^{-14}$ |
| L-HBr | 309 | 0.40 | 343 | 110.12 | | | 16.96 | $6.18 \times 10^{-14}$ |
| L-hemisulfate | 305 | 0.37 | 491 | 103.85 | 376 | 82.65 | 16.96 | $9.88 \times 10^{-14}$ |
| L-di(dihydrogen phosphate) | 308 | 0.43 | 454 | 96.80 | | | 5.99 | $6.68 \times 10^{-10}$ |
| L-acetate | 229 | 0.68 | 320 | 115.55 | | | 3.17 | $1 \times 10^{-15}$ |
| L-dihydrogen citrate | 298 | 0.56 | | | | | 5.03 | $1.63 \times 10^{-13}$ |
| L-docusate | 252 | 0.35 | | | | | 7.88 | $1 \times 10^{-15}$ |
| L-hemisuccinate | 274 | 0.75 | 390 | 123.71 | | | 3.72 | $3.57 \times 10^{-14}$ |

ΔCP, jump in the heat capacity at Tg determined from TMDSC; Tg, glass transition temperature (from standard DSC, heating rate 10K/min); Tm, melting temperature; ΔHm, enthalpy of fusion; Tc, temperature of crystallization onset; ΔHc, enthalpy of crystallization process. All these parameters were determined by means of DSC technique while σ dc(Tg) values were measured by means of dielectric spectroscopy. ΔpKa, defined as pKa (base) − pKa(acid), was calculated using ACD/ChemSketch version 12.0. The dielectric and calorimetric data for lidocaine HCl were taken from ref 33.

**Supporting Information**

## SI SYNTHESIS OF THE EXAMINED IONIC CONDUCTORS:

Lidocaine hydrobromide**:** Lidocaine base (Sigma-Aldrich, Germany) was dissolved in diethyl ether (Chromasolv, Germany) containing 0.25% v/v of purified water and purged with anhydrous hydrogen bromide gas obtained by titration of phosphorus pentoxide (Sigma-Aldrich, Germany) with concentrated (48%) hydrobromic acid (Sigma-Aldrich, Germany). White crystalline powder was isolated after an hour of stirring of precipitate at room temperature and washed with anhydrous diethyl ether. Lidocaine hemisulfate: Lidocaine base was dissolved at room temperature in ethyl acetate (Chromasolv, Germany) and combined with an equimolar amount of concentrated (95-98%) sulfuric acid (Sigma-Aldrich, Germany). A white, crystalline powder was isolated after an hour of stirring at room temperature and washed with ethyl acetate. Lidocaine di(dihydrogen phosphate)**:** This salt was obtained by a modified reaction crystallization method reported by Koehler and Hefferren (1964). Lidocaine base (Sigma-Aldrich, Germany) was dissolved at room temperature in anhydrous diethyl ether (Sigma-Aldrich, Germany). A white crystalline powder of the salt was precipitated by adding an excess of H3PO4 (85%, Riedel de Haen, Germany). The powder was washed with diethyl ether and dried. Lidocaine dihydrogen citrate**:** Equimolar amounts of lidocaine base and anhydrous citric acid (Sigma-Aldrich, Germany) were ground in an agate mortar with a drop wise addition of anhydrous ethanol (Fluka, Germany) until dissolved under a dry nitrogen purge. Ethanol was evaporated at room temperature under nitrogen bubble purge to a constant mass of the salt. Lidocaine hemisuccinate: Equimolar amounts of lidocaine base and succinic acid (Sigma-Aldrich, Germany) were ground in a mortar with a drop wise addition of an ethanol/acetone mix (1:1 v/v) and dried at room temperature to a constant mass under a dry nitrogen purge. Lidocaine docusate: Lidocaine hydrochloride monohydrate (Sigma-Aldrich, Germany) was combined in a mortar with a sodium docusate ethanolic solution. The suspension was evaporated to dryness using a Rotavapor R210 unit (Büchi, Switzerland) supplied with a heating bath B491 set to 50 ˚C under reduced pressure. The dry residue was reconstituted in dichloromethane. This suspension was filtered to isolate the solid residue of sodium chloride. The filtrate of lidocaine docusate was initially dried using the Rotavapor R210 unit (Büchi, Switzerland) at 50 ˚C under reduced pressure and then kept overnight at room temperature under a dry nitrogen purge. Lidocaine acetate: Lidocaine base was dissolved in concentrated (99.7%) acetic acid (Sigma-Aldrich, Germany). A white, crystalline precipitate

was formed and subsequently dried to evaporate excess of acetic acid under a dry nitrogen purge at room temperature.

## SII CALORIMETRIC EXPERIMENTS

The measurements and the data treatment methods are similar for all samples under investigation. Therefore, raw data and the corresponding data treatment will be shown for Lidocaine hemisuccinate alone.

The glass transition temperature *Tg* of the vitrification process (τα =100 - 1000 s) was determined as fictive temperature from the standard DSC scan on cooling or heating with 10 K/min scanning rate, an example is shown in Figure S1.

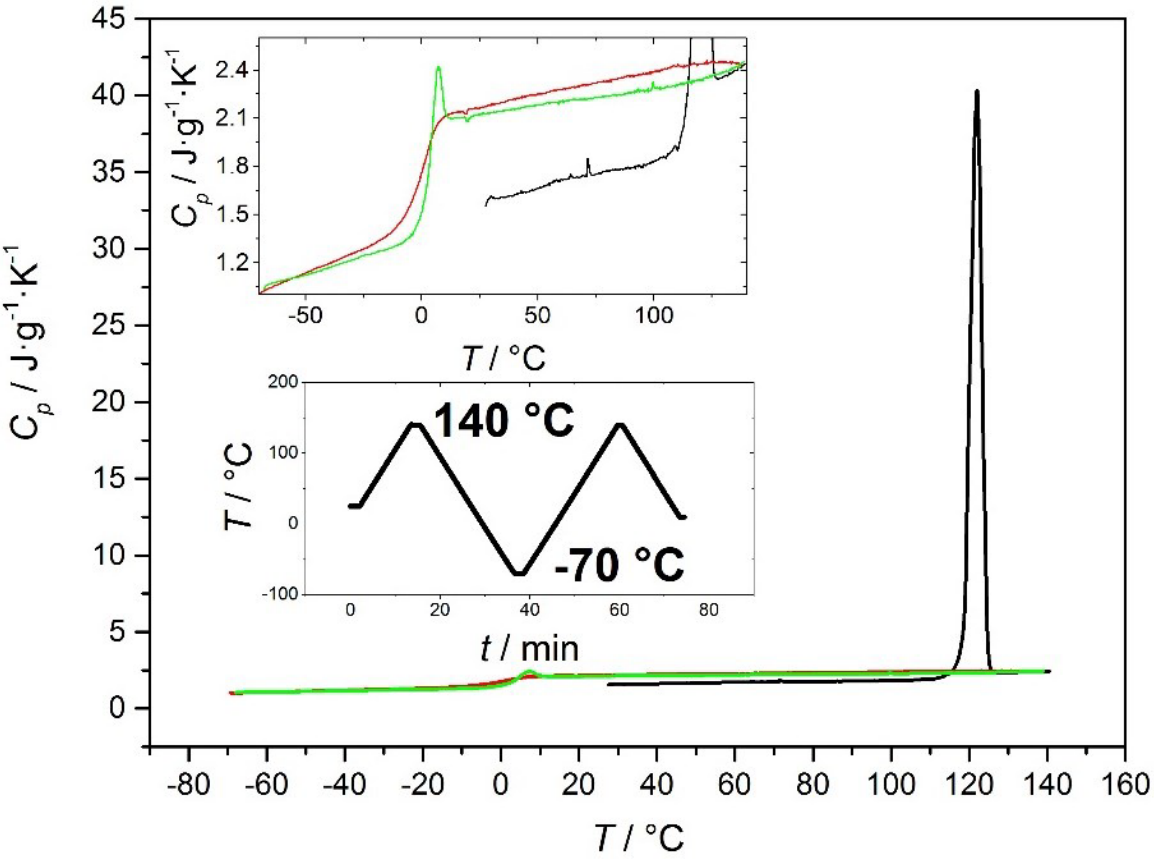


Figure S1 The sample was heated up to the melt at 140 °C (black curve), then cooled down to -70 °C with 10 K/min (red). The cooling scan shows a well pronounced vitrification step. Then the sample was heated up to 140 °C (green). The heating scan shows the glass transition step with an enthalpy relaxation peak. The upper inset shows a close up of the glass transition range on heating and cooling. The lower inset shows the temperature program.

The dynamic glass transition was investigated with two techniques on three devices. This is needed to cover the relaxation time range from vitrification ~1000 s to the shortest relaxation times of ~67 µs. With decreasing sample mass and measuring cell (addenda heat capacity), the shorter relaxation times could be probed.1

The temperature modulated DSC techniques were used in the PerkinElmer Diamond DSC and the Mettler Toledo Flash DSC 1.2 The first is a conventional DSC with sample mass in milligram range. The second, is also a differential calorimeter that uses a calorimetric chip as sample holder and measuring cell. In the conventional DSC samples were sealed in standard aluminum pans and in the Flash DSC the sample was placed directly in the middle of the sensor working area. A temperature program consisting of steps and isotherms was used for both devices. The step height, heating/cooling rate and especially the step duration, the isotherm, define the base frequency of the measurement. Figure S2 presents the response to such repeated steps. The glass transition is recognized from the measured heat flow signal between 100 and 150 min.

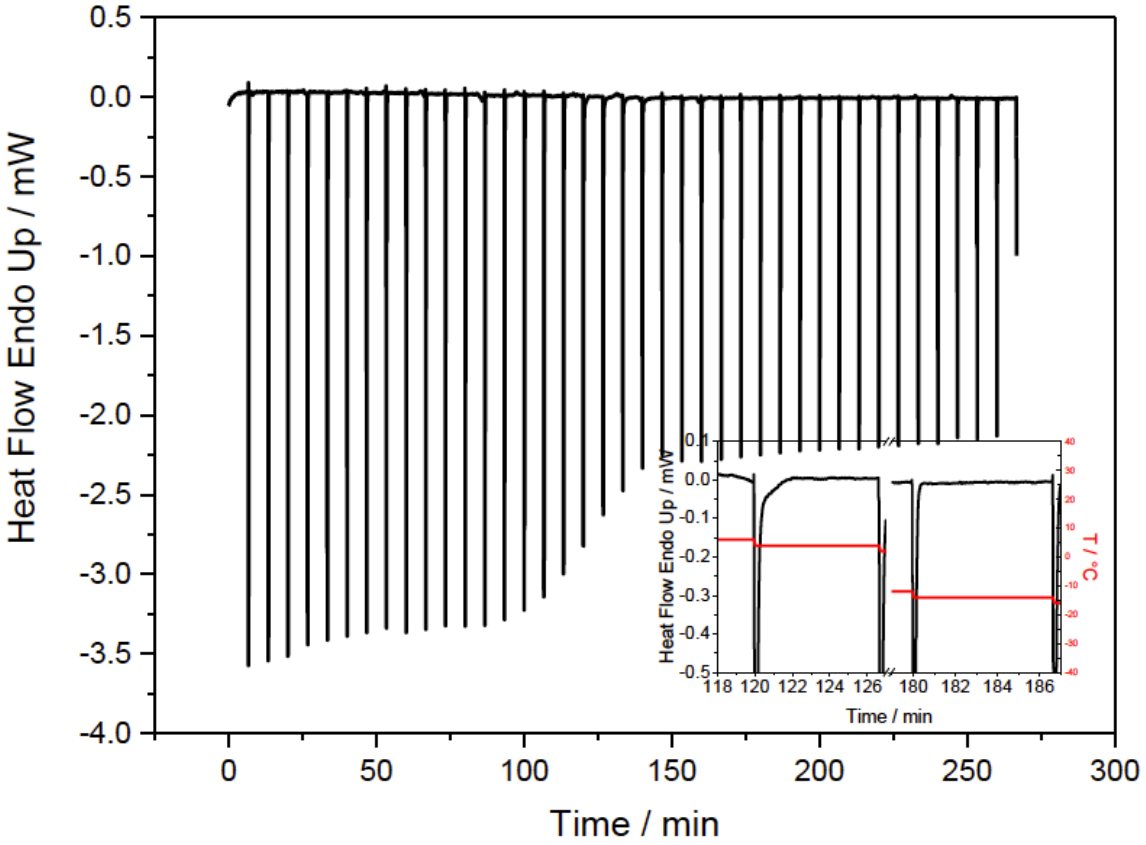


Figure S2 Heat flow as function of time in response to a step scan with steps of -2 K, cooling rate of 30 K·min-1 and isotherm duration of 6.6 min, corresponding to the base frequency *fth* = 0.0025 Hz (*ω0* = 0.0157 rad·s-1). The measurement was performed on a PerkinElmer

Diamond DSC with lidocaine succinate (*ms* = 5.4 mg). The inset shows the two steps after 120 and 180 min (5 °C and -13 °C respectively).

This heat flow versus time response (Figure S2) after Fourier transformation provides the complex heat capacity, *Cp(ω)*. The transformation for any frequency ω can be performed employing the following equation:

$$c_p(\omega) = \frac{1}{m_s} \frac{\sum_{i=1}^{n} \Phi_i \cos(\omega t_i) - i \sum_{i=1}^{n} \Phi_i \sin(\omega t_i)}{\sum_{i=1}^{n} \beta_i \cos(\omega t_i) - i \sum_{i=1}^{n} \beta_i \sin(\omega t_i)} \quad (1)$$

Where *ms* is sample mass, $\beta$ is heating rate and $\Phi$ is heat flow. In the resulting curves at the frequency dependent glass transition a step in the real part of complex heat capacity *C'p(ω)* and a peak in the imaginary part of complex heat capacity *C''p(ω) or the phase angle* appears, Figure S3. The angular frequency in equation 1 is chosen as $\omega = k \cdot \omega 0$ where *k* is an integer and *ω0* is the base frequency. This way the complex heat capacity at different frequencies is available from a single measurement.

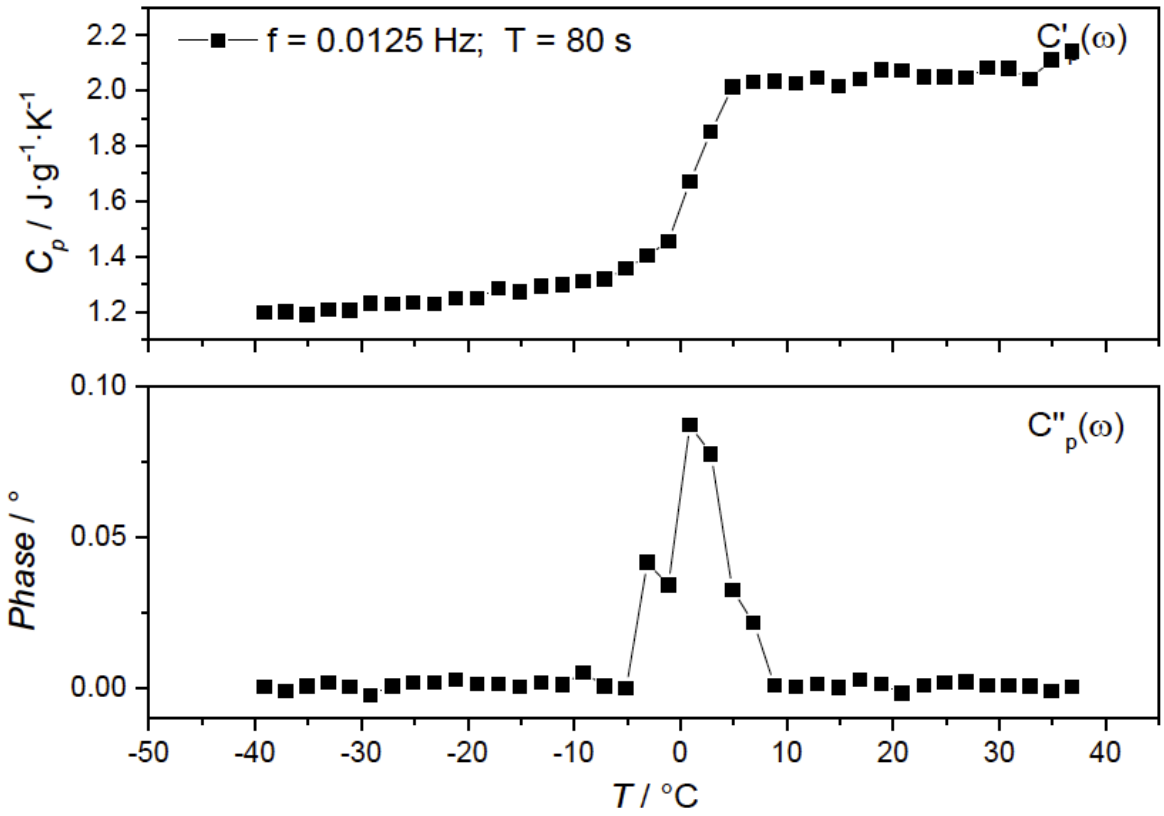


Figure S3 Complex heat capacity as obtained from equation 1 applied to the heat flow in Figure S2. The top part shows the step in the real part of the complex heat capacity and lower part the corresponding peak in the phase at the dynamic glass transition. The frequency corresponds to the fifth harmonic of the base frequency *ω0* and equals ω = 0.08 rad·s-1.

To find the dynamic glass transition temperature *Tg_dyn*(ω) one can fit a Gaussian to the phase angle and the peak position is the temperature of interest. Or, one can differentiate the real part of complex heat capacity and fit a Gaussian to find the deflection point that commonly correspond to the peak in the phase. We have used the second data treatment option, because the phase is not always that smooth and easy to handle. Frequency ω is converted to the structural relaxation time τ at *Tg, dyn*(ω) by τ = 1/ω, as common for dynamic experiments like dielectric spectroscopy.

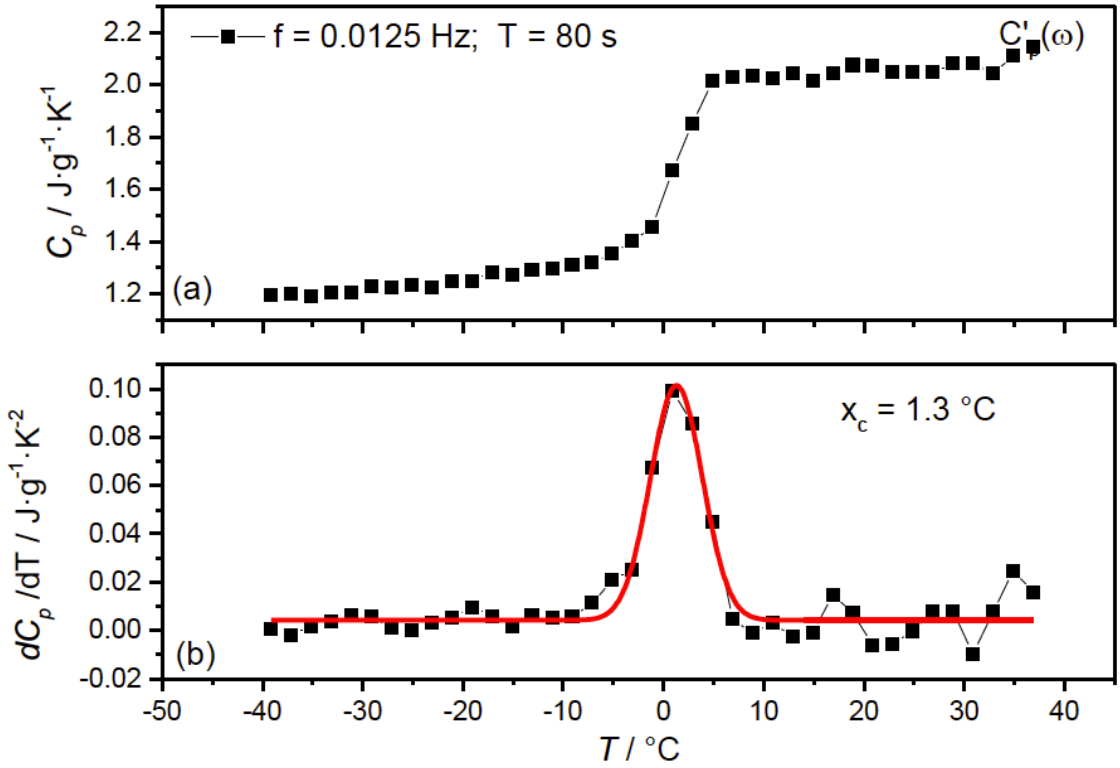


Figure S4 The upper plot represents the step in the real part of the complex heat capacity and the lower is its first order differential. The red curve is the fitted Gaussian.

The high frequency end of the data or short relaxation times, were acquired using an AC-chip calorimeter.3 In AC calorimetry an oscillating power is applied to the sensor heater and the corresponding temperature response is recorded. The heat capacity is again a complex function and under quasi adiabatic and quasi static conditions apparent heat capacity is given by

$$c_p(\omega) = \frac{\hat{P}}{\omega\hat{\Theta}} \quad (2)$$

Where the $\hat{P}$ is a power amplitude, $\omega$ is the frequency, and $\hat{\Theta}$ is the complex temperature amplitude. The raw data from AC-chip calorimeter is again a step in the real part of complex heat capacity and a peak in the phase.

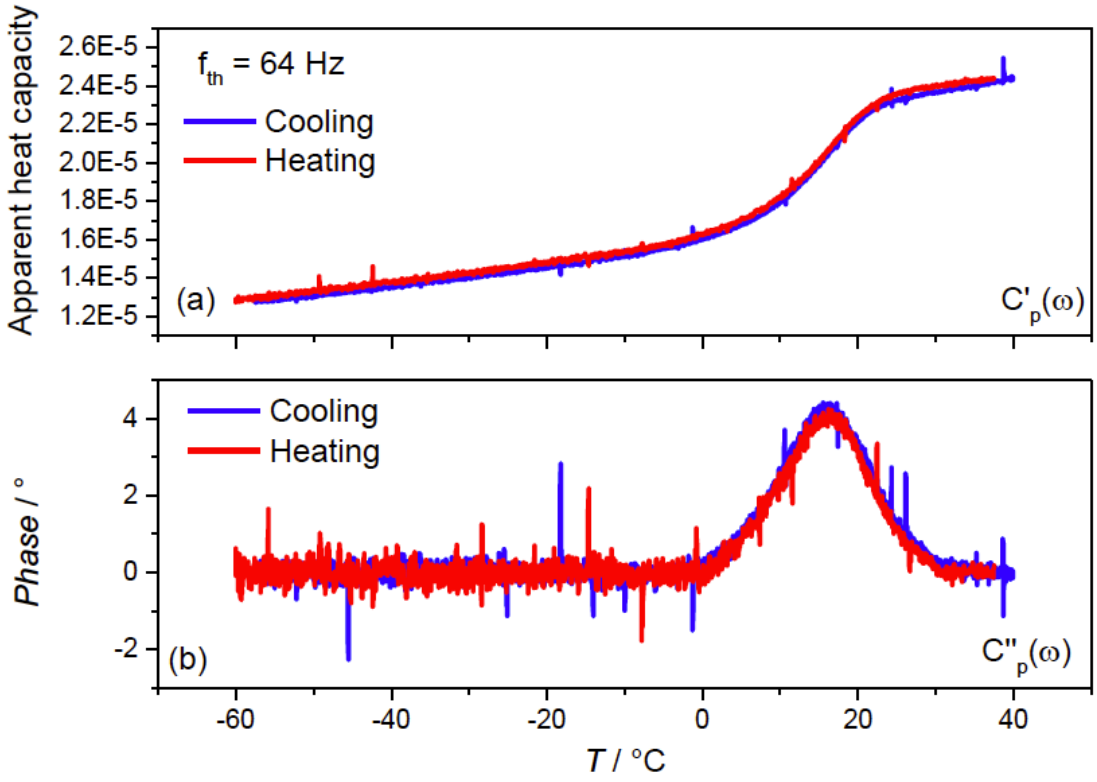


Figure S5 Top part: Magnitude of complex heat capacity (red curve on heating and blue on cooling). Lower part: Corresponding peak in the phase angle.

To find the dynamic glass transition temperature *Tg_dyn*(ω) one can fit a Gaussian to the phase angle and the peak position is the temperature of interest. Or, one can differentiate the real part of complex heat capacity and fit a Gaussian to find the deflection point that commonly correspond to the peak in the phase. We have used the second data treatment option, because the phase is not always that smooth and easy to handle.

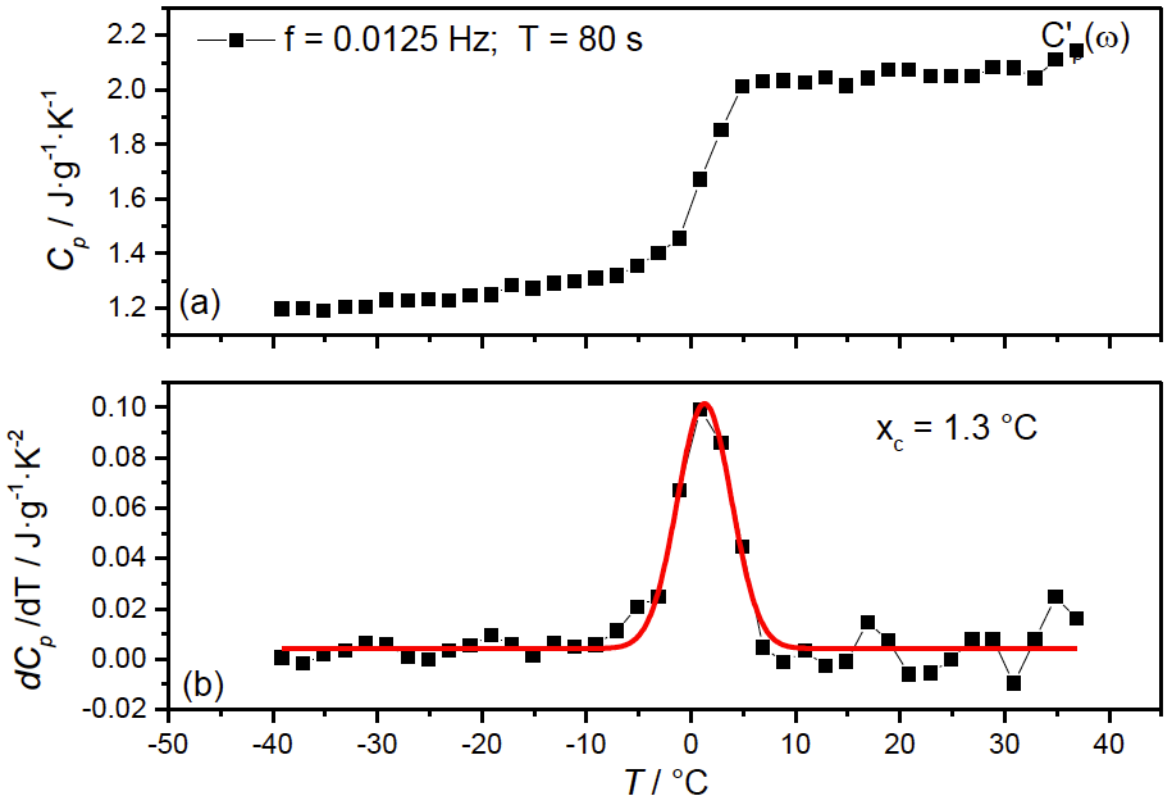


Figure S6 The upper plot represents the step in the real part of the complex heat capacity and the lower is its first order differential. The red curve is the fitted Gaussian.

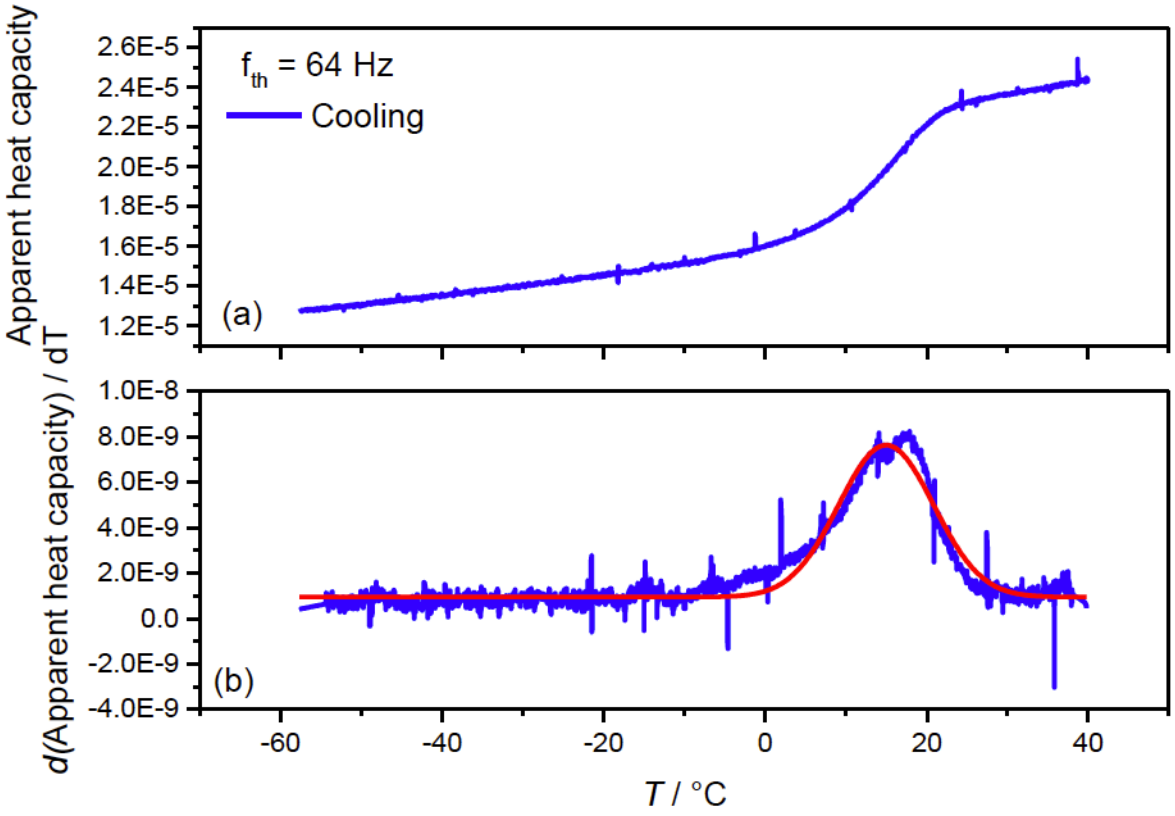


Figure S7 Top part is a step in an amplitude of the complex heat capacity (on cooling) and lower part is corresponding peak in phase (blue) and Gaussian fit (red curve). In difficult cases, it is needed to use a sum of two Gaussian to find precise peak position.

Temperature calibration for the different calorimeters was performed with different standards and results in an uncertainty of ±3 K for $Tg,dyn(\omega)$.

## SIII HYDROGEN BONDS NETWORK IN CRYSTAL STRUCTURES OF SELECTED LIDOCAINE SALTS

To visualize the H-bond network in hemisuccinate and di-(di-hydrogen phosphate) lidocaine salts the single crystal X-ray diffraction experiments have been performed.

SC-XRD data was collected on a Rigaku Saturn 724 CCD diffractometer (Tokyo, Japan) and Bruker Apex2 Duo (Billerica, MA, USA). Suitable crystals were selected and mounted using inert oil on a 0.30 mm quartz fibre tip and immediately placed on the goniometer head in a 150K nitrogen gas stream. Each data set was collected using Crystalclear-SM 1.4.0 software and 1680 diffraction images, of 0.5° per image, were recorded. Data integrations, reductions and corrections for absorption and polarization effects were all performed using Crystalclear-

SM 1.4.0 software. Space group determinations, structure solutions and refinements were obtained using Crystalstructure ver. 3.8 and Bruker Shelxtl ver. 6.14 software.

The crystallographic data was analysed in detail using: Mercury CSD 3.3.1 software, Ortep-34, Platon5 and CrystalExplorer (ver.3.0, Wolff et al., 2012) software. Crystallographic information files (CIFs) are available online free of charge from Cambridge Crystallographic Data Centre:

http://www.ccdc.cam.ac.uk/Community/Requestastructure/Pages/Requestastructure.aspx as: CCDC 935178 and CCDC 935179.

Crystal structures of lidocaine salts, diphosphate and hemisuccinate (Figure S8) may indicate where potential hydrogen bond interactions may occur in amorphous materials. In case of both salts lidocaine molecules do not form direct hydrogen bonds among each other. In the crystal structure of lidocaine di-(dihydrogen phosphate), cations form hydrogen bonds through oxygen (acceptor) and imine group (donor) of amide moiety (see Table 1 and Figure S10) as well as through nitrogen (acceptor) of diethyl imine moiety. In contrast to lidocaine di-(dihydrogen phosphate), in crystal lattice of lidocaine hemisuccinate oxygen of carbonyl group is not involved in formation of hydrogen bond network (Table S1, Figure S9), however it cannot be excluded that such a hydrogen bond structure exists in the amorphous state. In general, both lidocaine salts have rich hydrogen bond networks favouring hydrogen bond-based proton transfer in the amorphous form.

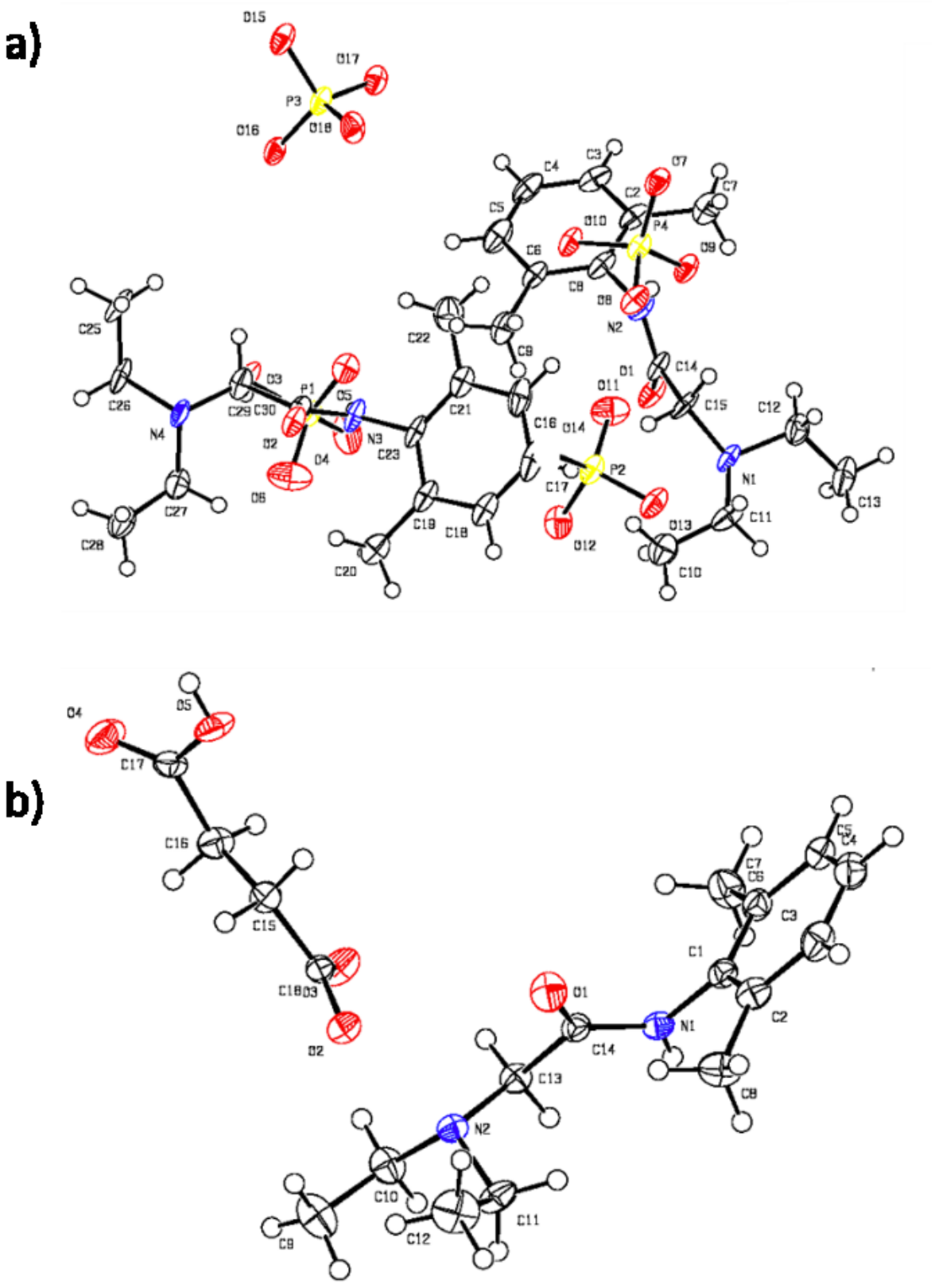


Figure S8 Ortep plot with 50% probability ellipsoids of: a) lidocaine diphosphate and b) lidocaine hemisuccinate.

Table S1. Hydrogen bonds networks in crystal structures of lidocaine di-(dihydrogen phosphate) (excluding phosphate-phosphate and phosphate-carbonyl interactions) and lidocaine hemisuccinate.

| **Lidocaine di-(dihydrogen phosphate)** | | | | | |
|---|---|---|---|---|---|
| **Nr** | **Donor-H...Acceptor** | **D – H (Å)** | **H...A (Å)** | **D...A (Å)** | **D - H...A (Å)** |
| 1a. | **N(2) --H(2) ..O(9)** | 0.86 | 1.94 | 2.785(8) | 168 |
| 2a. | **N(3) --H(3) ..O(5)** | 0.86 | 2.08 | 2.920(8) | 163 |
| 3a. | **C(4) --H(4) ..O(2)$^{(2)}$** | 0.93 | 2.55 | 3.314(9) | 139 |
| 4a. | **C(10) --H(10A) ..O(12)** | 0.96 | 2.43 | 3.273(9) | 147 |
| 5a. | **C(11) --H(11A) ..O(15)$^{(3)}$** | 0.97 | 2.49 | 3.308(8) | 142 |
| 6a. | **C(12) --H(12A) ..O(14)$^{(1)}$** | 0.97 | 2.54 | 3.269(9) | 132 |
| 7a. | **C(15) --H(15A) ..O(9** | 0.97 | 2.47 | 3.221(8) | 135 |
| 8a. | **C(15) --H(15B) ..O(11)** | 0.97 | 2.57 | 3.305(8) | 132 |
| 9a. | **C(20) --H(20A) ..O(2)** | 0.96 | 2.58 | 3.240(8) | 126 |
| 10a. | **C(28) --H(28A) ..O(16)$^{(4)}$** | 0.96 | 2.52 | 3.351(9) | 145 |
| Symmetry coordinates: 1. 1-x,1-y,-1/2+z; 2. x,1+y,z; 3. 1/2+x,1-y,z; 4. x,-1+y,z. | | | | | |
| **Lidocaine hemisuccinate** | | | | | |
| 1. | **N(1)-H(1)...O(2)$^{(1)}$** | 0.86 | 1.96 | 2.820(4) | 176 |
| 2. | **O(5)-H(5)...O(3)$^{(4)}$** | 0.82 | 1.79 | 2.583(5) | 162 |
| 3. | **C(5)-H(5A)...O(5)$^{(3)}$** | 0.93 | 2.60 | 3.488(5) | 161 |
| 4. | **C(8)-H(8C)...O(1)** | 0.96 | 2.43 | 3.183(6) | 136 |
| 5. | **C(13)-H(13A)...O(4)$^{(2)}$** | 0.97 | 2.39 | 3.324(5) | 161 |
| 6. | **C(13)-H(13B)...O(1)$^{(1)}$** | 0.97 | 2.59 | 3.374(5) | 138 |
| 7. | **C(15)-H(15A)...O(5)** | 0.97 | 2.47 | 2.804(5) | 100 |
| Symmetry coordinates: 1. 1-x,-1/2+y,1/2-z; 2. 2-x,-1/2+y,1/2-z; 3. -1/2+x,3/2-y,1-z; 4. 2-x,1/2+y,1/2-z. | | | | | |

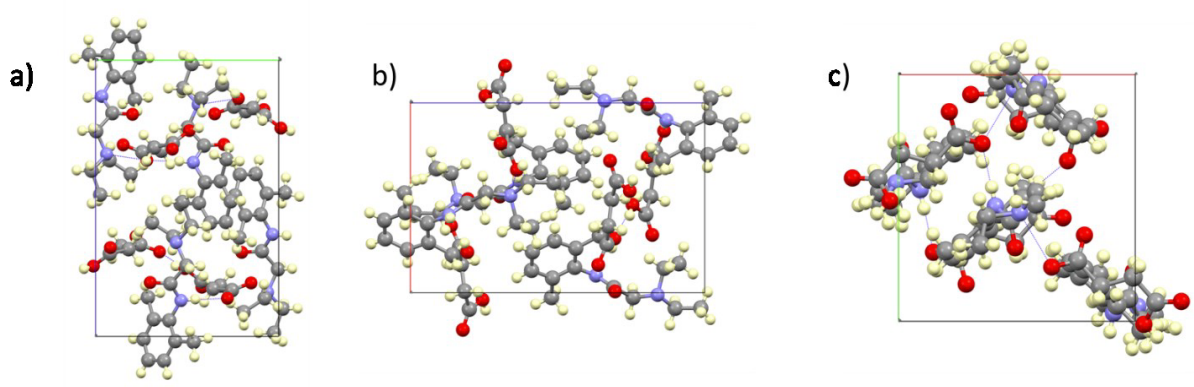


Figure S9. Crystal cell packing and hydrogen bonds network of lidocaine hemisuccinate along: a) a axis, b) b axis and c) c axis.

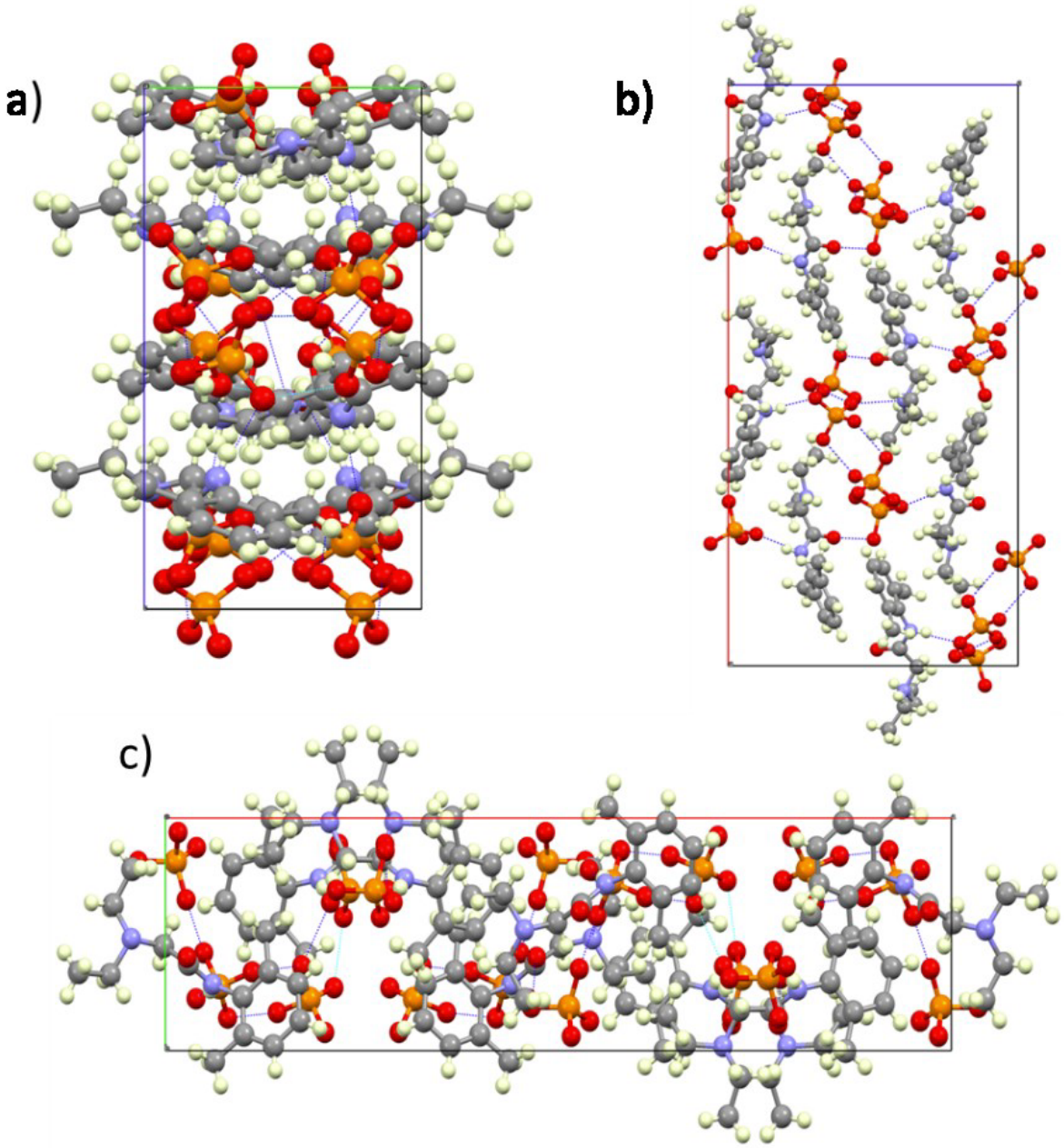


Figure S10 Crystal cell packing and hydrogen bonds network of lidocaine diphosphate along: a) a axis, b) b axis and c) c axis.

**REFERENCES FOR SUPPLEMENTAL INFORMATION**

1 Chua, Y.; Schulz, G.; Shoifet, E.; Huth, H.; Zorn, R.; Schmelzer, J. W. P.; Schick, C. *Colloid & Polymer Sci* **2014**, *292*, 1893-1904.

2 (a) Shoifet, E.; Chua, Y. Z.; Huth, H.; Schick, C., *Rev. Sci. Instr*. **2013**, *84*, 7, 073903-12.

(b) Ahrenberg, M.; Shoifet, E.; Whitaker, K. R.; Huth, H.; Ediger, M. D.; Schick, C. *Rev. Sci. Instr*. **2012**, *83*, 3, 033902-12.

3 Huth, H.; Minakov, A.; Schick, C. *Netsu Sokutei* **2005**, *32*, 2, 70-76.

4 Farrugia, L.J. *J. Appl. Crystallogr*. **1997**, *30*, 565.

5 Spek, A.L. *J. Appl. Crystallogr*. **2003**, *36*, 7-13.